

Photodissociation of CBrCl_3 at 234 and 265 nm: Evidence of the curve crossing

Young-Jae Jung, Moon Soo Park, Yong Shin Kim^{a)}, and Kyung-Hoon Jung^{b)}
Center for Molecular Science and Department of Chemistry, Korea Advanced Institute of Science and Technology, Taeduck Science Town, Taejon 305-701, Korea

Hans-Robert Volpp
Physikalisch-Chemisches Institut der Universität Heidelberg, Im Neuenheimer Feld 253, D-69120 Heidelberg, Germany

(Received 17 May 1999; accepted 9 June 1999)

The photodissociation dynamics of CBrCl_3 was studied near 234 and 265 nm using a two-dimensional photofragment ion imaging technique. Bromine fragments monitored in this study were produced via direct dissociation of CBrCl_3 , represented by $\text{CBrCl}_3 \rightarrow \text{CCl}_3 + \text{Br}(^2P_{1/2})/\text{Br}(^2P_{3/2})$. The branching ratio of $\text{Br}(^2P_{1/2})$ (denoted Br^*)/ $\text{Br}(^2P_{3/2})$ (denoted Br) showed strong excitation energy dependence. The product quantum yields at two different excitation wavelengths were $\Phi_{234 \text{ nm}}(\text{Br}^*) = 0.31 \pm 0.01$ and $\Phi_{265 \text{ nm}}(\text{Br}^*) = 0.68 \pm 0.02$, respectively. The speed and angular distributions of Br^* and Br fragments were determined. Similar values of $\beta(234 \text{ nm}) = -0.44$ and $\beta(265 \text{ nm}) = -0.47$ for Br were observed, while β values for Br^* were found to be markedly different, $\beta(234 \text{ nm}) = -0.34$ and $\beta(265 \text{ nm}) = 1.43$. The strong curve crossing, $^1Q_1 \rightarrow ^3Q_0$, and the angular distribution of Br^* suggesting a typical perpendicular transition, were observed at 234 nm photodissociation. © 1999 American Institute of Physics. [S0021-9606(99)02533-7]

I. INTRODUCTION

Alkyl halide undergoes direct dissociation of the C–X (X=Cl, Br, I) bond via $\sigma^* \leftarrow n$ transition of lone pair electrons of X at its first absorption A-band.^{1–3} Since the properties related to the transition are preserved due to its short dissociation time, the observed properties of the products (i.e., the vector quantities, internal energy distributions, and branching ratios of various product states) reflect the related potential energy surface.

Atomic bromine exhibits a 40 times more powerful atmospheric ozone depletion potential⁴ than a chlorine atom.⁵ In this regard, bromine containing compounds (e.g., CH_3Br , CD_3Br , CF_3Br , and CBrCl_3) have attracted a great deal of attention among environmental scientists to investigate the environmental impacts of these compounds in recent years.^{6–10} CBrCl_3 reveals its absorption maxima at 130, 180, and 240 nm^{11–13} and its A-band center near 240 nm, and a large absorption cross section at even 280 nm.¹¹ Two peaks in the vacuum ultraviolet (VUV) region were assigned to Rydberg transitions of atomic bromine. The CBrCl_3 , a precursor of Br and CCl_3 ,¹⁴ therefore, renders itself to be an ideal system to study excitation energy dependence and to set up an excited potential surface related to photolysis on the energy compared to CY_3Br (Y=H, D, F) of which A-band absorption is centered near 200 nm. Gas-phase photodecomposition studies of CBrCl_3 at 365 nm were carried out under static conditions using stable end-product analysis

(CBr_2Cl_2 , C_2Cl_6 , Br_2 , and CCl_4) and it was suggested that two different excited states may be involved in the $\text{CCl}_3 + \text{Br}$ primary fragmentation process.¹⁵ CCl radicals were detected in flash photolysis studies of CBrCl_3 in the wavelength region of 160–200 nm and it was concluded that CCl is formed via the unimolecular decomposition of vibrationally excited CCl_3 .¹⁶ In VUV photolysis experiments using H atom Lyman- α (121.6 nm) and Ar I resonance lines (104.8 and 106.7 nm) electronically excited CCl_2 radicals in the \tilde{A}^1B_1 state were observed and $\text{CCl}_2(\tilde{A}) + \text{BrCl}$ and $\text{CCl}_2(\tilde{A}) + \text{Br} + \text{Cl}$ product formation channels were proposed.¹² A rotatable quadrupole mass spectrometer experiment revealed that after CBrCl_3 photoexcitation at 248 nm the primary dissociation process leads exclusively to CCl_3 and Br^* products. For this product channel an anisotropy parameter of -0.4 ± 0.2 was obtained and it was proposed that the fragmentation process involves simple C–Br bond scission.⁹ In the 193 nm CBrCl_3 photolysis using the same technique, besides the $\text{CCl}_3 + \text{Br}$ product channel, the $\text{CCl}_2\text{Br} + \text{Cl}$ product channel formation was observed with a relative yield of $\text{Br} : \text{Cl} = 7 : 3$. Based on the measured product anisotropy parameters, $\beta = 1.3$ for Br and $\beta = -0.2$ for Cl , direct dissociation mechanism was proposed.¹⁰ Additional Br fragments formation from the unimolecular decay of the internally excited CCl_2Br was also observed in the study. However, in the 248 and 193 nm experiments direct distinction between Br and Br^* fragments was not possible.

R–Br has shown many similarities with R–I in its physical and chemical properties. The major differences between R–Br and R–I are the bond dissociation and spin–orbit coupling energies, E_{soI} . Due to the larger bond dissociation en-

^{a)}Present address: Electronics and Telecommunications Research Institute, Taeduck Science Town, Taejon 305-350, Korea.

^{b)}Author to whom correspondence should be addressed; electronic mail: khjung@hanbit.kaist.ac.kr

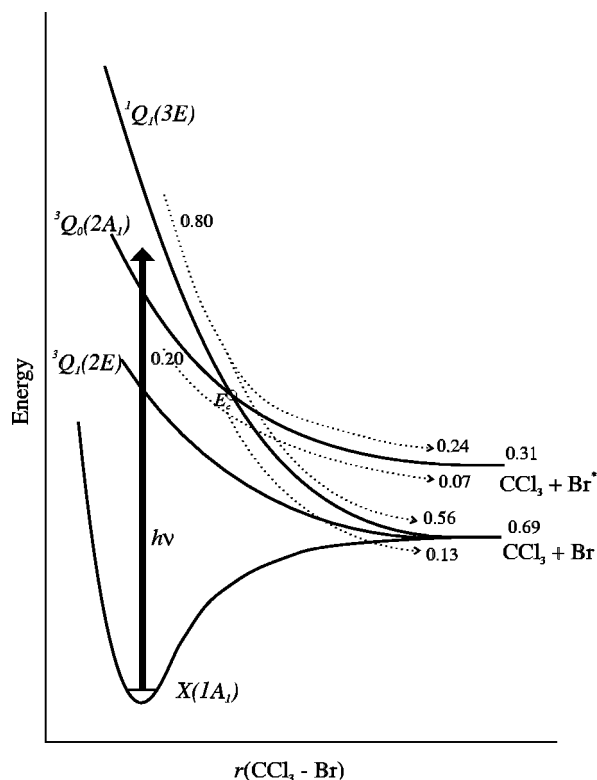


FIG. 1. One-dimensional schematic representation of the potential energy curves involved in the CBrCl_3 photodissociation in the A-band.

energy of C–Br compared to that of the C–I bond, R–Br shows a blue shift in A-band absorption. Because E_{s0} , 44 kJ/mol, for bromine¹⁷ is smaller than that of iodine, 91 kJ/mol, the spin selection rule, $\Delta S=0$, is more strictly observed in the case of R–Br than R–I. Three dissociative excited states in the A-band of alkyl halides via overlap electronic transitions^{18,19} are represented by the ${}^3Q_1(2E)$, ${}^3Q_0(2A_1)$, and ${}^1Q_1(3E)$ in Mulliken's notation²⁰ and illustrated in Fig. 1. The 3Q_0 potential energy surface is responsible for Br^* formation with the parallel transition, while the 3Q_1 and 1Q_1 surfaces correlate Br formation with the perpendicular transition character.

In 193 nm photolysis of CH_3Br ,⁶ the curve crossing from the 3Q_0 to the 1Q_1 surface has been barely observed with a rotatable quadrupole mass spectrometer. In 210 nm studies of CH_3Br and CD_3Br via the photoimaging technique,⁷ Br^* fragments have shown $\cos^2\theta$, while Br fragments have been more isotropic and contained a $\sin^2\theta$ angular component. The curve crossing from the 3Q_0 to the 1Q_1 surface has been observed qualitatively. In 193 nm CF_3Br photolysis,⁸ Br^* fragments have shown mixed characteristics of parallel and perpendicular transitions with a ratio of 1.3:1, while Br fragments have a strong parallel transition character. This indicates that Br fragments mostly originate from initial excitation of the 3Q_0 surface, while Br^* fragments result from initial excitations of the 3Q_0 and 1Q_1 surfaces with similar contribution. Because of this finding, a new potential energy surface with C_s symmetry has been suggested. As a consequence, the curve crossing probability is found to depend on the physical and chemical properties of CY_3 (Y=H, D, F). The CBrCl_3 photodissociation study,

therefore, serves in aiding the understanding of the curve crossing phenomenon related to the replacement of (Y=H, D, F) to Cl.

In this work we report the photodissociation dynamics of CBrCl_3 on photoexcitation energy dependencies utilizing the photoimage technique coupled with resonance enhanced multiphoton ionization (REMPI) at 234 and 265 nm.

II. EXPERIMENT

The photofragment image system used in this study has been described previously in detail.²¹ A sample mixture was prepared with 10 torr CBrCl_3 seeded in 1.5 atm helium and injected into the reaction region using a molecular beam valve (General valve), pulsed at 10 Hz. The CBrCl_3 (Aldrich, purity >97%) was used after several freeze–thaw cycles with no further purification.

A linear polarized UV laser light (typically 60 $\mu\text{J}/\text{pulse}$), generated by doubling the output of Nd:YAG (355 nm) pumped dye laser and aligned by using a half-wave retardation plate, was focused perpendicularly onto the ionization zone of the molecular beam with a 150 mm focal length lens and parallel to an image plane. The CBrCl_3 was photolyzed by the UV laser light and bromine atom fragments were then selectively ionized at 233.9 and 264.8 nm for Br^* , and at 233.6 and 264.9 nm for Br using the [2+1] REMPI technique²² within the same laser pulse. The laser was scanned over a range of 4 cm^{-1} in order to detect all velocity component of bromine fragments.

Bromine fragment ions were accelerated to the repelling plate with positive high voltage and then passed through an extract and ground plates with a 20 mm diameter hole which caused the nonhomogeneous electric field around the electrode.²³ The bromine ion cloud was then expanded spherically due to not only the recoil velocity of the fragments but also the nonhomogeneous electric field. The expansion rate was calibrated against the known values in Br_2 and I_2 photolyses. The expanded ion cloud of bromine was projected onto a two-dimensional position-sensitive detector plate which consists of a microchannel plate (MCP)/phosphor screen (Galileo, FM2040) and a charge coupled device (CCD) camera (photometric, CH250). A negative high voltage pulse with 150 ns duration was applied to MCP to separate the bromine ion signal from those of scattered laser light and background ions with different masses. The image was summed from over 10 000 shots or more and the background was removed by subtracting a reference image collected at an off-resonant wavelength under the same conditions. The REMPI time-of-flight (TOF) mass spectra were acquired using a photomultiplier tube (Hamamatu, 1P21) instead of the CCD camera.

III. RESULT AND ANALYSIS

A. Time-of-flight mass spectra

1. 234 nm

Figure 2 shows TOF mass spectra of photofragments of CBrCl_3 in the range of $m/e=0-250$ a.u. at Br [2+1] REMPI wavelength. Seven peaks were found at $m/e=12$, 35, 37, 47, 49, 79, and 81, respectively. The $m/e=79$ and 81

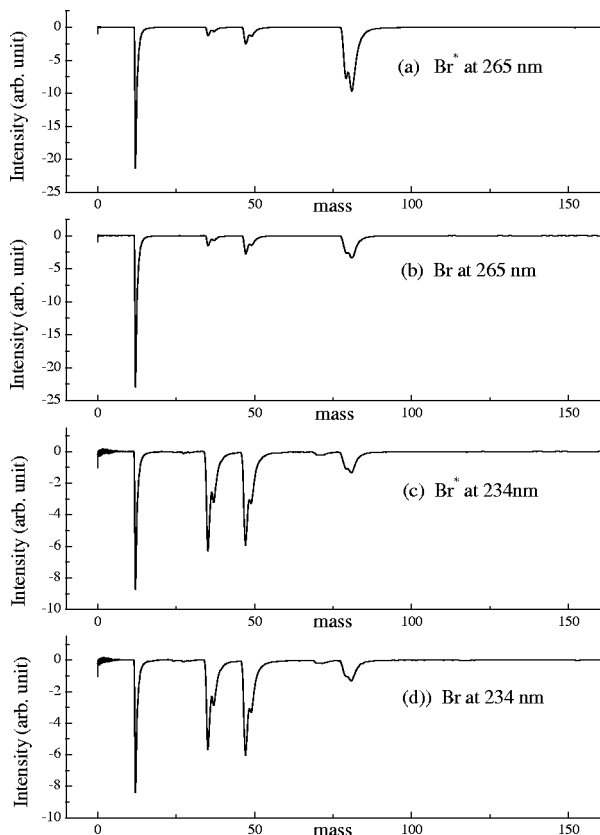


FIG. 2. Time-of-flight mass spectra of photofragments in the m/e range 0–250 obtained in the 265 nm [(a), (b)] and 234 nm [(c), (d)] photolyses of CBrCl₃. The signals at $m/e = 79$ and 81 originate from $^{79}\text{Br}^+$ and $^{81}\text{Br}^+$ ions formed by the [2+1] REMPI process while the other peaks result from ions generated by nonresonant ionization.

peaks represent $^{79}\text{Br}^+$ and $^{81}\text{Br}^+$ ions formed via [2+1] REMPI, while the rest of the peaks result from nonresonance ionization processes. The $m/e = 12, 35, 37, 47,$ and 49 peaks are assigned to be $^{12}\text{C}^+, ^{35}\text{Cl}^+, ^{37}\text{Cl}^+, ^{12}\text{C}^{35}\text{Cl}^+,$ and $^{12}\text{C}^{37}\text{Cl}^+$, respectively.

2. 265 nm

The $\text{C}^+, \text{Cl}^+, \text{CCl}^+,$ and Br^+ ions were observed in TOF mass spectra of CBrCl₃ at Br [2+1] REMPI wavelength and displayed in Fig. 2. The TOF mass spectra in 265 nm photodissociation is similar to that in 234 nm except for the intensities. The intensity of Cl^+ in 234 nm photolysis is bigger than that in 265 nm suggesting that this is because of either an increase of atomic chlorine formation or an improvement of the nonresonance MPI efficiency of the atomic chlorine. The smaller the difference between the current wavelength and the Cl [2+1] REMPI wavelength becomes, the higher the nonresonance MPI efficiency of atomic chlorine becomes.²⁴ Used Br [2+1] REMPI wavelengths, 233.6 nm for Br and 233.9 nm for Br*, are closely located at Cl [2+1] REMPI wavelength, 235.1 nm for Cl* and 235.3 nm for Cl. Another cause of the intensity change of Cl^+ is an increase in atomic chlorine from photodissociation of the C–Cl bond. Excitation of the C–Cl local bond at 265 nm has not been reported yet but it occurs at 234 nm.^{9,10}

B. Relative quantum yields

The ratio $N(\text{Br}^*)/N(\text{Br})$ is proportional to the measured ion signal ratio in TOF mass spectra by the equation,

$$\frac{N(\text{Br}^*)}{N(\text{Br})} = k \frac{S(\text{Br}^*)}{S(\text{Br})}, \quad (1)$$

where $N(i)$ is the number of species i , $S(i)$ the measured intensity of species i , and k the proportionality constant. The k value is determined by the relative detection efficiency of Br* and Br and the instrument factor, and was obtained from Br₂ photolysis under the same experimental condition. The ratios of $N(\text{Br}^*)/N(\text{Br})$ at 234 and 265 nm photolyses were found to be 0.45 ± 0.04 and 2.16 ± 0.22 , respectively. The k values at 234 and 265 nm photolyses were 0.42 ± 0.02 and 0.73 ± 0.02 , respectively. The intensity of species i was integrated over Doppler width and probe laser band width to acquire $S(i)$ from scanned TOF mass spectra.

From the calculated ratios, the relative quantum yields of $\Phi(\text{Br}^*)$ and $\Phi(\text{Br})$ were determined by the relation

$$\Phi(\text{Br}^*) = \frac{N(\text{Br}^*)}{N(\text{Br}^*) + N(\text{Br})}, \quad \text{and} \quad \Phi(\text{Br}) = 1 - \Phi(\text{Br}^*). \quad (2)$$

The relative quantum yields $\Phi(\text{Br}^*)$ are determined to be 0.31 ± 0.01 at 234 nm and 0.68 ± 0.02 at 265 nm photolyses, respectively.

C. Speed and angular distribution

Br* and Br images at 234 and 265 nm are displayed in Fig. 3. The shape of the images reveals the speed and angular distributions of the photofragments. These raw images are two-dimensional projections of three-dimensional speed and angular distributions of bromine fragments. The Br* image at 265 nm displays a typical polar cap appearance, characteristic of $\cos^2 \theta$ distribution, while that of Br at 265 nm shows an equatorial belt appearance, characteristic of $\sin^2 \theta$ distribution. The formations of Br* and Br atoms are therefore correlated with several channels according to the difference between the angular distributions of these images. In 234 nm photodissociation, both images of Br* and Br fragments have equatorial belt appearances as shown in Fig. 3. The image of Br fragments in 234 nm photodissociation has very similar angular distribution to that in 265 nm photodissociation, while the image of Br* fragments in 234 nm photolysis differs from that in 265 nm.

A two-dimensional raw image with cylindrical symmetry around the polarization axis of the photolysis laser has been used to reconstruct a three-dimensional velocity distribution²⁵ by performing an inverse Abel transformation.²⁶ Since the inverse Abel transformation is very sensitive to noise, the raw images have been presmoothed with the Gaussian filter with a 5×5 window and the standard deviation of 2 in a pixel unit typically to reduce the noise effect on the transformation. Due to the cylindrical symmetry of velocity distribution, every planar slice containing the symmetry axis is equivalent to reconstructed images.

By integrating the reconstructed three-dimensional speed distribution over all angles at each speed, the speed distribu-

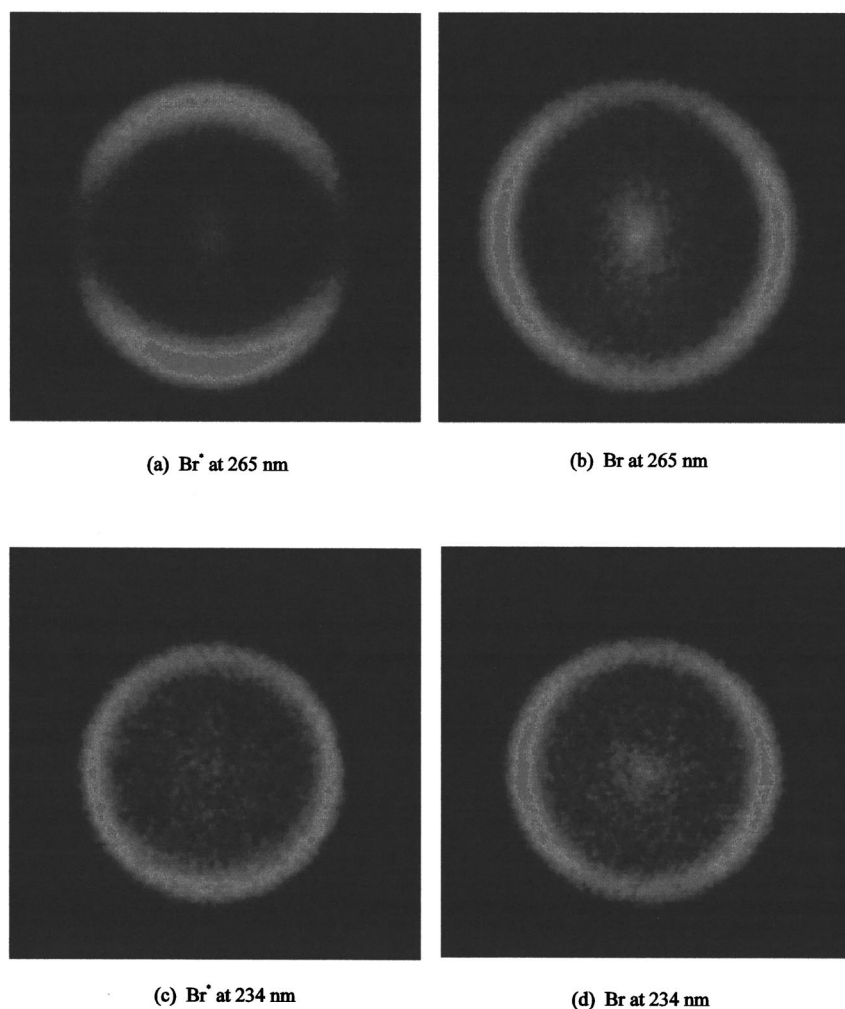


FIG. 3. Raw ion images of Br* and Br fragments from the photolysis of CBrCl₃ at 265 nm [(a), (b)] and 234 nm [(c), (d)]. In all images the linear polarization vector of photolysis laser is vertical.

tion $P(v)$ has been obtained as shown in Fig. 4. The center-of-mass translational energy distribution, $P(E)$, has been estimated from the speed distribution by the equation

$$P(E) = P(v) \frac{dv}{dE}. \quad (3)$$

The internal energy of the CCl₃ radical, E_{int} , is calculated using an energy conservation relationship

$$E_{\text{ava}} = h\nu - D_0 + E_{\text{int}}^P, \quad (4)$$

$$E_{\text{int}} = E_{\text{ava}} - E_t - E_{\text{el}}, \quad (5)$$

where $h\nu$ is the photon energy (512 kJ/mol at 234 nm and 452 kJ/mol at 265 nm), $D_0 = 230.2$ kJ/mol, the dissociation energy of CCl₃-Br at 0 K,²⁷ E_{int}^P the internal energy of CCl₃-Br, and E_{el} the electronic energy level of atomic bromine. The E_{int}^P is assumed to be zero in the supersonic molecular beam condition, E_{el} , 0 kJ/mol for Br and 44 kJ/mol for Br*. The translation energies E_t and E_t/E_{ava} are listed in Table I.

The angular distribution $P(\theta)$ in Fig. 5 has been obtained by integrating the reconstructed three-dimensional speed distribution over a proper range of the speed at each angle, where θ is the angle between the laser polarization axis and the recoil velocity of photofragments. In order to

estimate an anisotropy parameter β , the angular distribution $P(\theta)$ has been fitted into the standard formula²⁸

$$P(\theta) = 1 + \beta P_2(\cos \theta), \quad (6)$$

where $P_2(\cos \theta)$ is the second-order Legendre polynomial. The anisotropy parameter, β values of Br* and Br images at 234 and 265 nm photolyses are listed in Table I.

IV. DISCUSSION

In 265 nm photolysis of CBrCl₃, Br* fragments have shown a strong parallel angular distribution, while Br fragments show a perpendicular one. These findings imply that the major parts of Br* fragments originate from initial excitation of the ³Q₀ surface and some via the curve crossing from the ¹Q₁ to the ³Q₀ surface whereas Br fragments mostly result from initial excitations of the ¹Q₁ and ³Q₁ surfaces and some via the curve crossing from the ³Q₀ to the ¹Q₁ surface. The photodissociation dynamics of CBrCl₃ at 265 nm has shown a very similar pattern to that of CH₃Br at 193 nm in the point of lower curve crossing probability.

The angular distribution of Br fragments in 234 nm photolysis of CBrCl₃ reveals a perpendicular transition, implying that the major portion of Br fragments originate from the ¹Q₁ surface. The angular distribution of Br* fragments in

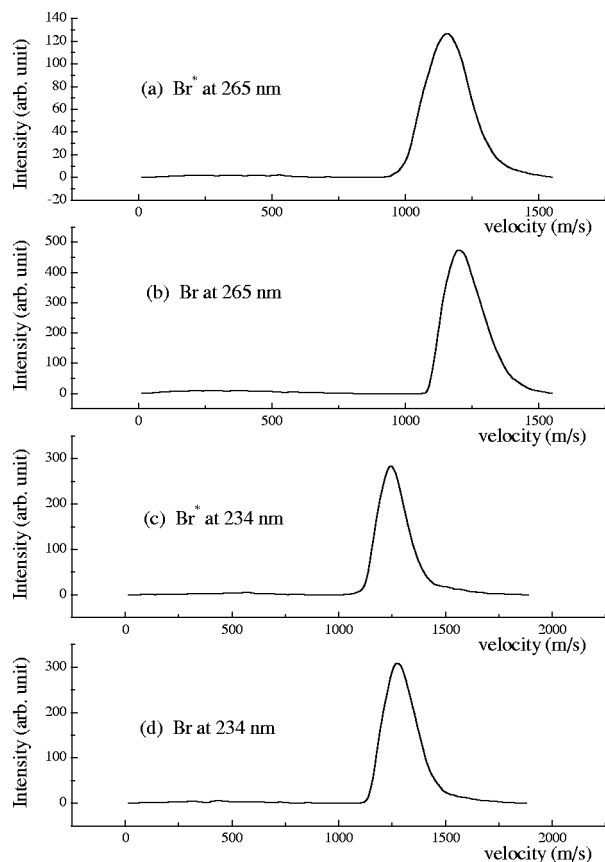


FIG. 4. The speed distribution of the Br^* and Br fragments for the 265 nm [(a), (b)] and 234 nm [(c), (d)] photolysis wavelength.

234 nm, a typical perpendicular transition, indicates that Br^* fragments are mostly via curve crossing from the 1Q_1 to the 3Q_0 surface, and the rest are from initial excitation of the 3Q_0 surface. Br^* fragments are formed less than Br fragments in 234 nm CBrCl_3 photolysis, while the branching ratio of Br^* in 265 nm photolysis is more than that of Br. This finding indicates that the transition to the 3Q_0 surface is a main one in 256 nm photolysis because of the less probable curve crossing from the 1Q_1 to 3Q_0 surface. The large formation of Br in 234 nm indicates that the 1Q_1 and 3Q_1 surfaces are main contribution. Because the 1Q_1 and 3Q_1 surfaces are split above and below the 3Q_0 surface, the main contribution in 265 nm photolysis, the large formation of Br fragments in 234 nm photolysis is not caused by the large

TABLE I. The energy and angular distribution of bromine fragments.

Wavelength		$h\nu$ kJ/mol	E_{ava} kJ/mol	E_t kJ/mol	FWHM kJ/mol	β	E_t/E_{ava}
265 nm	Br^*	451.6	221.3	89.2	18.4	1.43	0.40
	Br	451.8	221.5	97.8	16.4	-0.47	0.44
248 nm ^a	Br^*	482.4	252.0				
	Br	482.4	252.0	83.7	33.2	-0.4	0.33
234 nm	Br^*	512.3	281.9	107.6	16.3	-0.31	0.38
	Br	512.1	281.7	113.8	18.5	-0.44	0.40
193 nm ^b	Br^*	619.8	389.4	71.2	58.6	1.3	0.18
	Br	482.4	389.4				

^aFrom Ref. 9.

^bFrom Ref. 10.

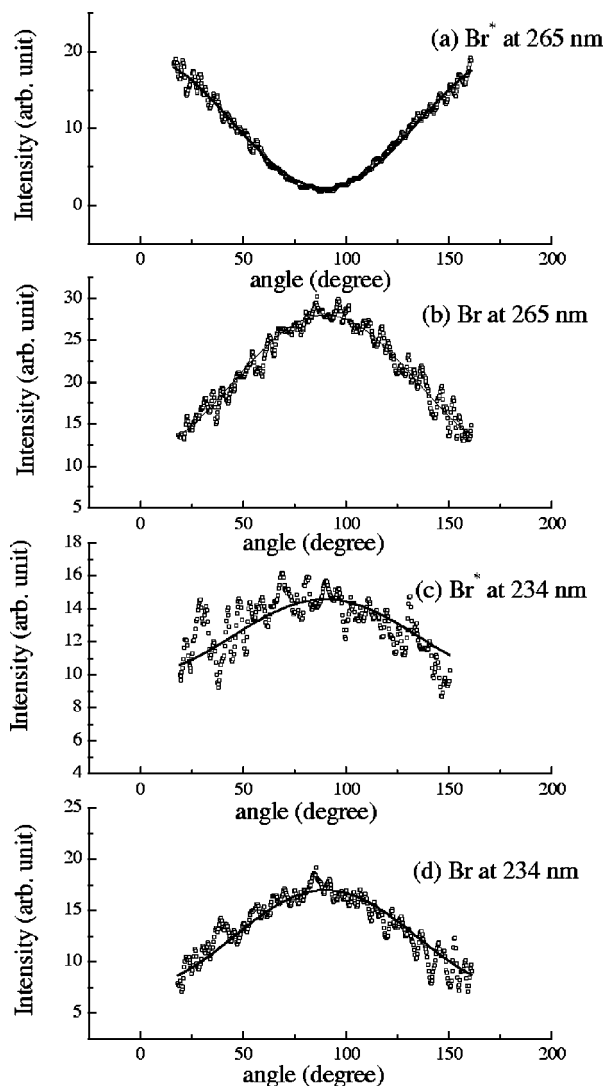


FIG. 5. The angular distribution of the Br^* and Br fragments for the 265 nm [(a), (b)] and 234 nm [(c), (d)] photolysis wavelength.

absorption of the 3Q_0 but of the 1Q_1 . From the relative quantum yield, we suggest that the 1Q_1 and 3Q_0 surfaces are involved and 3Q_1 surface is eliminated in 234 nm photolysis.

After excitation at 234 nm, $\beta = -0.31$ for Br^* and $\beta = -0.44$ for Br were observed. These results are in agreement with earlier 248 nm photodissociation studies⁹ in which $\beta = -0.4$ was reported. In the studies it was found that in contrast to the integrated intensities the shape of the product translational energy distribution, which represents a superposition of the translational energy distributions of Br^* and Br fragments, was independent of the photolysis laser polarization direction. This observation indicates that after excitation at 248 nm, in agreement with the present result at 234 nm, similar angular distribution of Br^* and Br fragments occurs. In the case when the recoil velocity and angular distribution difference between Br^* and Br fragments is small,^{9,10} it becomes very difficult to resolve them in the rotatable quadrupole mass spectrometry. Since the mass spectrometry has the limit of separation between Br^* and Br, the photoimage technique coupled with REMPI is more appropriate to measure

TABLE II. Contribution ratio of the parallel and perpendicular transition.

Wavelength			⊥
265 nm	Br*	0.81	0.19
	Br	0.18	0.82
234 nm	Br*	0.23	0.77
	Br	0.19	0.81

the recoil velocity of the fragments Br* and Br distinguishably in R-Br photolyses.^{9,10,29-31}

In earlier studies of methyl halide photodissociations,^{1-3,6-10} the perpendicular transition of X* (X=I and Br) fragments has not been observed. In CY₃I (Y=H, D, F) photolyses, the formation of I* fragments from the curve crossing from the ¹Q₁ to the ³Q₀ surface are smaller than that from the ³Q₀ surface because an absorption of the ³Q₀ surface is much larger than that of the ¹Q₁ and the ³Q₀ surfaces.¹⁸ Then the angular distribution of I* fragments must have the characteristic of the parallel transition. Despite the ¹Q₁ and the ³Q₀ surfaces' similar contribution to the A-band in the case of the CY₃Br (Y=H, D, F) photodissociation, the energy level of the ¹Q₁ surface, which is too high, makes the formation of Br* fragments more difficult from the curve crossing from the ¹Q₁ to the ³Q₀ surface than from initial excitation of the ³Q₀ surface. In 234 nm photolysis of CBrCl₃, Br* fragments, resulting from perpendicular transition, are observed due to its unique photolysis behavior.

In order to estimate the relative contributions of the parallel, and perpendicular components to Br* and Br fragments formation channels, the classical relationship was used.

$$\beta = x_{||}\beta_{||}^{\text{eff}} + x_{\perp}\beta_{\perp}^{\text{eff}}, \quad \text{and } x_{||} + x_{\perp} = 1, \quad (7)$$

where $\beta_{||}^{\text{eff}}$ and $\beta_{\perp}^{\text{eff}}$ represent effective anisotropy parameters for parallel and perpendicular transitions which account for the anisotropy reduction due to the finite parent molecule rotational temperature. For $\beta_{||}^{\text{eff}}$ a value of 1.8 was used which represents the average value we measured from the anisotropy parameters in CF₃I at 308 and 277 nm³¹ under experimental conditions similar to those of the present study. At CF₃I photolysis wavelength, I* fragments formation originates entirely from a parallel transition (³Q₀←X) followed by a direct dissociation, which makes it an ideal reference system. For $\beta_{\perp}^{\text{eff}}$ a value of $-\frac{1}{2} \times \beta_{||}^{\text{eff}} = -0.9$ was used, assuming that the anisotropy reduction is the same for the parallel and perpendicular component. The $x_{||}$ and x_{\perp} values for Br* and Br fragments formation channels, respectively, are listed in Table II.

The curve crossing has been estimated usually from the relative quantum yield and angular distribution of ground state X in CY₃X photolysis. Because of the small contribution of the ³Q₁ surface and the absence of the ¹Q₁ surface in the red edge of the A-band of CY₃I, the formation of I fragments directly correlates to the curve crossing from the ³Q₀ to the ¹Q₁ surface,³² and the curve crossing from the ¹Q₁ to the ³Q₀ surface can be ignored.

$$\Phi(\text{I})\Sigma \propto \text{Probability}({}^3Q_0 \rightarrow {}^1Q_1), \quad (8)$$

TABLE III. The relative fraction of each potential surface at 265 and 234 nm.

Wavelength		Initial excitation	Curve crossing
265 nm	Br*	³ Q ₀	¹ Q ₁ → ³ Q ₀
		0.55	0.13
	Br	¹ Q ₁ + ³ Q ₁	³ Q ₀ → ¹ Q ₁
		0.26	0.06
234 nm ^a	Br*	³ Q ₀	¹ Q ₁ → ³ Q ₀
		0.07	0.24
	Br	¹ Q ₁	³ Q ₀ → ¹ Q ₁
		0.56	0.13

^aThe probability of the curve crossing, $P({}^3Q_0 \rightarrow {}^1Q_1) = 0.13 / (0.13 + 0.07) = 0.65$ and $P({}^1Q_1 \rightarrow {}^3Q_0) = 0.24 / (0.24 + 0.56) = 0.30$ were calculated from the result at 234 nm.

where Σ , the fraction of I fragments via the curve crossing from ³Q₀ to the ¹Q₁ surface to overall I fragments, can be estimated from the angular distribution of I fragments. Meanwhile in CY₃Br photolysis,⁸ because both the curve crossing from the ³Q₀ to the ¹Q₁ surface and its reverse have been observed considerably, the fraction of Br* fragments, formed via the crossing from the ¹Q₁ to the ³Q₀ surface, to overall Br* fragments is a good measure for estimating the curve crossing.

The curve crossing probability is estimated qualitatively by the Landau-Zener equation:³³

$$P = 1 - \exp\left(\frac{-4\pi^2 V_{12}^2}{h|\Delta F|v_c}\right) \quad (9)$$

and

$$v_c = \sqrt{\frac{2(h\nu - E_c)}{\mu}}, \quad (10)$$

where V_{12} is the coupling term between the diabatic potentials, $|\Delta F|$ the difference in diabatic force at the curve crossing point, v_c the relative velocity between two fragments through the point, E_c the potential energy at the point, and μ the reduced mass. If the Landau-Zener model is valid, the curve crossing probability from the ³Q₀ to the ¹Q₁ surface is the same as its reverse from the ¹Q₁ to the ³Q₀ surface. But the estimated probability of the curve crossing from the ³Q₀ to the ¹Q₁ surface is higher than that of the reverse in this study as listed in Table III. This disagreement, the limit of the Landau-Zener model, may have resulted from the difference between the shapes of the two-dimensional potential surface of the ³Q₀ and ¹Q₁. Though the Landau-Zener model holds for the diatomic molecules, it does not for the polyatomic molecules because of its one-dimensional potential surface model. To explain the discrepancy from the Landau-Zener model in CY₃I photolysis,³⁴ the distortion of the C_{3v} symmetry of CY₃I via ν_6 , an e-type bending vibration, has been suggested to accommodate the finding.³⁵

Two-dimensional potential surfaces of the excited state of CH₃I have been calculated as C_s symmetry and indicated that V_{12} , the coupling term, is a function of ϕ , where ϕ is the bending angle of the CH₃-I bond in Fig. 6.³⁵ The one-dimensional Landau-Zener model does not describe multi-dimensional surfaces well for polyatomic molecule. CBrCl₃

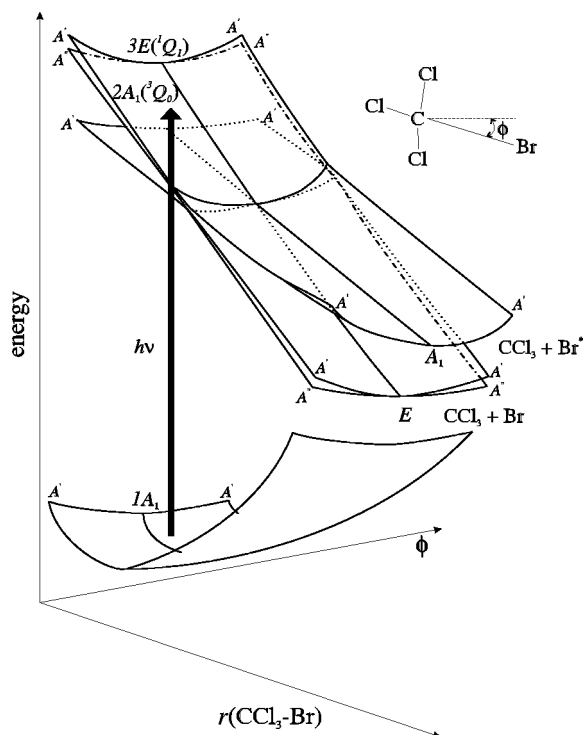
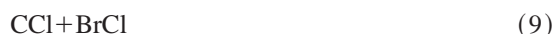
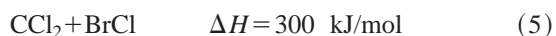
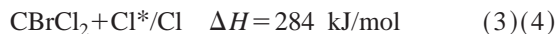


FIG. 6. Two-dimensional schematic representation of the CBrCl₃ potential energy surfaces for linear and bent dissociation pathways.

has been treated using the same analogy of that in CH₃I. According to the potential surface of CH₃I, the ¹Q₁ surface is steeper than the ³Q₀ surface to both the *r*(C–Br) and ϕ axis. Then the wavefunction of the excited electron in the ¹Q₁ surface has a narrower distribution to the ϕ axis than that in the ³Q₀ surface of CBrCl₃. Since CBrCl₃ in the ³Q₀ surface has a strong distortion from the C_{3v} symmetry due to the broader distribution of wavefunction to the ϕ axis but in the ¹Q₁ surface retains the C_{3v} symmetry well, the probability of the curve crossing from the ¹Q₁ to the ³Q₀ surface becomes lower than its reverse. Another reason for the small probability of the curve crossing from the ¹Q₁ to the ³Q₀ surface, is the shorter dissociation times of the ¹Q₁ surface than that of the ³Q₀ surface, which results from the greater steepness of the ¹Q₁ surface to the *r*(C–Br) axis than that of the ³Q₀ surface. CBrCl₃ in the ¹Q₁ surface has a shorter residence time to distort the C_{3v} symmetry than that in the ³Q₀ surface.

In TOF spectra at 234 and 265 nm in Fig. 2, C⁺, Cl⁺, and CCl⁺ fragments are resulted from either nonresonance ionization or secondary dissociation. The possible dissociation channels are¹¹



Since an anomalous velocity distribution of bromine fragments, resulting from the secondary dissociation (8), has not been observed in the image, we suggest that the dissociation (8) occurs very rarely. Formation of the CCl₂ radical in CBrCl₃ photolysis has been studied detecting the fluorescence of CCl₂(\tilde{A}) \rightarrow CCl₂(X).¹¹ Because the CCl₃ radical has not enough internal energy to break the CCl₂–Cl bond, the CCl₂ radical must absorb additional photons to form an electronically excited CCl₂ state and to break the CCl₂–Cl bond. A reaction mechanism is suggested as a explanation for the formation of C⁺, Cl⁺, and CCl⁺ by nonresonance ionization.



From nonactual observations of CCl₃⁺ and CCl₂⁺ ions, it is suggested that all CCl₃ and CCl₂ radicals may either undergo dissociation by an additional photon or by excess internal energy, or remain free causing the nonresonance multiphoton ionization (MPI). If C⁺, Cl⁺, and CCl⁺ ions originate from C, Cl, and CCl neutral radicals, these species must exhibit very small peaks because of very low efficiency of the nonresonance MPI of C, Cl, and CCl radicals like CCl₃ and CCl₂ radicals. Accordingly, we conclude that C⁺, Cl⁺, and CCl⁺ ions result from the heterogeneous dissociation of CCl₂ as the suggested mechanism. It is necessary for the CCl₂ radical to absorb several photons to dissociate heterogeneously. The electronically excited CCl₂ radical is known to have an abnormally large absorption cross section¹¹ which agrees well with this work.

ACKNOWLEDGMENTS

The authors gratefully acknowledge the Korea Research Foundation for its support of this research by the Korea-Germany Joint Project, 1998–2001. H-R. Volpp would also like to thank Professor J. Wolfrum, Director of the Institute of Physical Chemistry, University of Heidelberg, for his continuous support and stimulating discussions.

¹S. M. Penn, C. C. Hayden, K. J. Carlson Muyskens, and F. F. Crim, *J. Chem. Phys.* **89**, 2909 (1988).

²D. W. Chandler, J. W. Thoman, Jr., M. H. M. Janssen, and D. H. Parker, *Chem. Phys. Lett.* **156**, 151 (1989).

³Y. S. Kim, W. K. Kang, D-C. Kim, and K-H. Jung, *J. Phys. Chem. A* **101**, 7576 (1997).

⁴R. P. Wayne, *The Chemistry of Atmospheres*, 2nd ed. (Oxford University, New York, 1991), and references therein.

⁵S. C. Wofsy, M. B. McElroy, and Y. L. Yong, *Geophys. Res. Lett.* **2**, 125 (1975).

⁶G. N. A. Van Veen, T. Baller, and A. E. De Vries, *Chem. Phys.* **92**, 59 (1985).

⁷W. P. Hess, D. W. Chandler, and J. W. Thoman, Jr., *Chem. Phys.* **163**, 277 (1992).

⁸M-A. Thelen and P. Felder, *Chem. Phys. Lett.* **204**, 135 (1996).

⁹Y. R. Lee, W. B. Tzeng, Y. J. Yang, Y. Y. Lin, and S. M. Lin, *Chem. Phys. Lett.* **222**, 141 (1994).

¹⁰Y. R. Lee, Y. J. Yang, Y. Y. Lin, and S. M. Lin, *J. Chem. Phys.* **103**, 6966 (1995).

¹¹P. Cadman and J. P. Simon, *Faraday Trans. Soc.* **62**, 631 (1966).

- ¹²T. Ibuki, N. Takahashi, A. Hiraya, and D. Shobatake, *J. Chem. Phys.* **85**, 5717 (1986).
- ¹³C. Roxlo and A. Mandl, *J. Appl. Phys.* **51**, 2969 (1980).
- ¹⁴J. J. Russeli, J. A. Seetula, D. Gutman, F. Danis, F. Caralp, P. D. Lightfoot, R. Lesclaux, C. F. Melius, and S. M. Senkan, *J. Phys. Chem.* **94**, 3277 (1990).
- ¹⁵H. W. Sidebottom, J. M. Tedder, and J. C. Walton, *Faraday Trans. Soc.* **65**, 755 (1969).
- ¹⁶J. P. Somons and A. J. Yarwood, *Faraday Trans. Soc.* **59**, 90 (1963).
- ¹⁷R. H. Garstang, *J. Res. Natl. Bur. Stand.* **68A**, 61 (1964).
- ¹⁸A. Gedanken and M. D. Rowe, *Chem. Phys. Lett.* **34**, 39 (1975).
- ¹⁹W. S. Felps, J. D. Scott, and S. P. McGlynn, *J. Chem. Phys.* **104**, 419 (1996).
- ²⁰R. S. Mulliken, *J. Chem. Phys.* **8**, 382 (1940).
- ²¹W. K. Kang, Y. S. Kim, and K-H. Jung, *Chem. Phys. Lett.* **244**, 183 (1995).
- ²²M. S. Park, S. H. Lee, and K-H. Jung (unpublished).
- ²³A. T. J. B. Eppink and D. H. Parker, *Rev. Sci. Instrum.* **68A**, 3477 (1997).
- ²⁴S. L. Chin and P. Lambropoulos, *Multiphoton Ionization of Atoms* (Academic, Canada, 1984).
- ²⁵Details about image reconstruction can be found, e.g., in D. W. Chandler, T. N. Kitsopoulos, M. A. Buntine, D. P. Baldwin, R. I. McKay, A. J. R. Heck, and R. N. Zare, in *Gas Phase Chemical Reaction Systems*, edited by J. Wolfrum, H.-R. Volpp, R. Rannacher, and J. Warnatz (Springer, New York, 1996).
- ²⁶S. M. Candel, *IEEE Trans. Acoust., Speech, Signal Process.* **29**, 963 (1981).
- ²⁷G. D. Mendenhall, D. M. Golden, and S. W. Benson, *J. Phys. Chem.* **77**, 2707 (1973).
- ²⁸R. N. Zare and D. R. Herschbach, *Proc. IEEE* **51**, 173 (1964).
- ²⁹L. J. Butler, E. J. Hints, S. F. Shane, and Y. T. Lee, *J. Chem. Phys.* **86**, 2051 (1987).
- ³⁰S. Das and D. J. Tannor, *J. Chem. Phys.* **91**, 2324 (1989).
- ³¹Y. S. Kim, W. K. Kang, and K-H. Jung, *J. Chem. Phys.* **105**, 551 (1996).
- ³²S. Uma and Puspendu Kumar Das, *Chem. Phys. Lett.* **241**, 335 (1995).
- ³³L. D. Landau and E. M. Lifshitz, *Quantum Mechanics 3* (Pergamon, New York, 1977), p. 347.
- ³⁴M. D. Person, P. W. Kash, and L. J. Butler, *J. Chem. Phys.* **94**, 2557 (1991).
- ³⁵S. Yabushita and K. Morokuma, *Chem. Phys. Lett.* **153**, 517 (1988).